ISSN 1063-7842, Technical Physics, 2013, Vol. 58, No. 1, pp. 105–110. © Pleiades Publishing, Ltd., 2013.
Original Russian Text © V.O. Vas'kovskii, P.A. Savin, S.O. Volchkov, V.N. Lepalovskii, D.A. Bukreev, A.A. Buchkevich, 2013, published in Zhurnal Tekhnicheskoi Fiziki, 2013, Vol. 83, No. 1, pp. 110–116.

PHYSICS OF LOW-DIMENSIONAL STRUCTURES

Nanostructuring Effects in Soft Magnetic Films and Film Elements with Magnetic Impedance

V. O. Vas'kovskii[a], P. A. Savin[a], S. O. Volchkov[a], V. N. Lepalovskii[a] *, D. A. Bukreev[b], and A. A. Buchkevich[a]

[a] *Ural Federal University, pr. Lenina 51, Yekaterinburg, 620002 Russia*
[b] *East Siberian State Academy of Education, Irkutsk, 664011 Russia*
e-mail: vladimir.lepalovskiy@usu.ru

Received February 28, 2012

Abstract—The magnetization reversal and magnetic impedance (MI) of films and film elements based on $Fe_{19}Ni_{81}$ and $Fe_{72.5}Cu_{1.1}Nb_{1.9}Mo_{1.5}Si_{14.2}B_{8.7}$ alloys with a varied thickness, heat-treatment temperature, and the number of thin Cu interlayers are studied. The dependences of the coercive force and the magnitude of MI on these parameters are found. Layered structuring is shown to be an effective method for improving the functional characteristics of MI elements. In elements containing nanocrystalline $Fe_{19}Ni_{81}$ layers, this is related to the restructuring of a magnetic structure; in elements containing amorphous $Fe_{72.5}Cu_{1.1}Nb_{1.9}Mo_{1.5}Si_{14.2}B_{8.7}$ layers, this improvement is likely to be caused by a decrease in the effective electrical resistivity.

DOI: 10.1134/S1063784213010222

INTRODUCTION

Magnetic impedance (MI) occupies a significant place among the physical effects that form the basis of modern magnetic sensorics [1–4]. This effect consists in a change of the impedance of a ferromagnetic conductor Z for a high-frequency alternating current in applied magnetic field H. MI depends on the excitation current parameters, the material properties, and the conductor geometry and becomes large when skin effect is strong, i.e. when the characteristic size of the sample is comparable to the skin depth. Therefore, the most favorable MI conditions take place in soft magnetic ribbons [5], wires [6], or films [7]. Such films have certain technological advantages in designing integrated magnetic sensors.

Classic permalloy is the most known soft magnetic material that retains its properties in a film state. However, the so-called supercritical state, which is characterized by a low magnetic permeability and, correspondingly, weak MI [8], can form in relatively thick films of this alloy, which are potentially more suitable for MI sensors. An amorphous FINEMET-type alloy is another widely used soft magnetic material: it is widely applied to produce melt-quenched ribbons with high MI [1]. Films of this alloy can also acquire the supercritical state [9].

The specific magnetic structure called as the supercritical state forms due to a certain compromise between shape anisotropy, which specifies the magnetization orientation in the film plane, and perpendicular magnetic anisotropy, which corresponds to the magnetization orientation along the normal to the film plane. Perpendicular magnetic anisotropy is often related to the so-called columnar microstructure forming in metallic films. Thus, the suppression of the supercritical state can be associated with the decomposition of the columnar structure, which seems to be possible when a base film is structured by layers of another material. Some data on layered structuring as a method for increasing the MI of soft magnetic film elements are presented in [9–12]. However, they are not systematic. The purpose of this work is to compare the magnetic properties of permalloy (PM) and FINEMET (FM) alloy films subjected to structuring by Cu layers and to study the MI of the film elements based on these films.

EXPERIMENTAL

Film samples were prepared by rf sputtering onto Corning glass substrates in homogeneous 100-Oe magnetic field H_t. The targets were made of alloys $Fe_{19}Ni_{81}$, $Fe_{72.5}Cu_{1.1}Nb_{1.9}Mo_{1.5}Si_{14.2}B_{8.7}$, and Cu. The working gas (Ar) pressure during sputtering was 2×10^{-1} Pa. The thickness of homogeneous films varied in the range 10–1000 nm. Samples 500 nm thick were additionally subjected to stepwise vacuum annealing at temperatures up to 500°C. The annealing time at each temperature was 1 h. The structured films were the layered systems in which magnetic layers of the same thickness alternated with 3-nm-thick Cu interlayers. The total magnetic layer thickness was fixed (500 nm) and the number of interlayers N was varied. To measure the magnetic properties of the films, we used a vibrating-sample magnetometer, a magneto-optical device, and a scanning magnetic-force microscope.

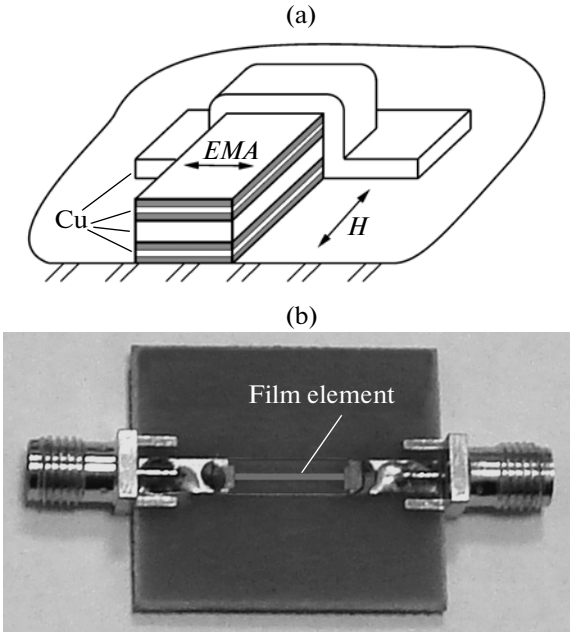

Fig. 1. (a) Schematic diagram of part of the film element and (b) photograph of the measuring cell.

We used a similar sputtering process to prepare the film elements used for MI investigations. In addition, to achieve a certain shape of the elements, we deposited materials through a mask with a rectangular 10.0 × 0.5-mm hole. Field H_t was oriented along the short side of the rectangle. Along the normal to the surface, the elements were as a three-layer sandwich in which outer 500-nm-thick layers were made of a magnetic material and the central layer had the same thickness and was made of copper. This configuration is considered to be most suitable to achieve high MI [13, 14]. In addition, as the films described above, the magnetic layers were subjected to fine structuring via the introduction of 3-nm-thick Cu interlayers. At the final stage of preparation, 2 × 2-mm copper bonding pads were applied onto the ends of the elements through a special-purpose mask. Figure 1a schematically shows the structure of the film elements. The impedance was measured on an Agilent E4991A high-frequency analyzer in a quasi-static varying magnetic field applied along the long side of the rectangle. To this end, we used a special measuring cell, whose photograph is shown in Fig. 1b. The bonding pads of the elements were glued to the bonding pads of the cell with a conducting glue.

RESULTS AND DISCUSSION

An analysis of the magneto-optical magnetization curves of one-layer samples with a relatively small thickness ($L < 200$ nm) shows that the films of both compositions have a uniaxial magnetic anisotropy and the easy magnetization axis (EMA) coincides with the axis of application of technological field H_t. The

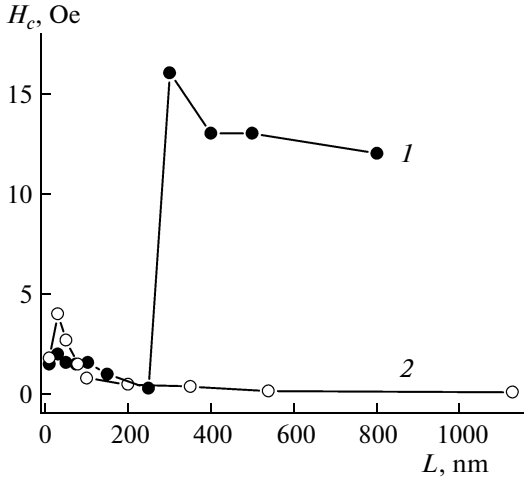

Fig. 2. Coercive force vs. the thickness of (*1*) $Fe_{19}Ni_{81}$ or (*2*) $Fe_{72.5}Cu_{1.1}Nb_{1.9}Mo_{1.5}Si_{14.2}B_{8.7}$ film.

anisotropy field in both cases is about 5 Oe. Figure 2 shows the dependence of coercive force H_c, the values of which were determined from longitudinal (measured along the EMA) magneto-optical hysteresis loops, on thickness L of PM and FM films. It is seen that both dependences have the same character at $L <$ 200 nm. Specifically, H_c increases as the thickness decreases to 30 nm, which is likely to be caused by an increase in the role of the surface relief in delaying the displacement of domain walls and by a change in the structure of the domain walls. Very thin films ($L \leq$ 10 nm) exhibit a tendency toward a decrease in the coercive force, which can result from certain defragmentation of magnetic deposits and the manifestation of superparamagnetic behavior of magnetization. However, the range of larger thicknesses is more important due to the MI effect. As follows from Fig. 2, the $H_c(L)$ dependences for two types of films differ radically in this range. In the PM films, the coercive force increases sharply (by an order of magnitude) to ~10 Oe at $L \sim 250$ nm, and this level is retained in thicker films. In contrast, H_c in the FM films decreases monotonically with increasing thickness: H_c becomes lower than 0.2 Oe at $L \geq 500$ nm. This difference can be related to the microstructures of the films, which lead to the difference in their magnetic anisotropies.

For comparison, Figs. 3a and 3c show the magnetometric longitudinal hysteresis loops of 500-nm-thick PM and FM films. The PM loop is seen to have (Fig. 3a) a broad central part and narrow skew regions preceding magnetic saturation. This is a typical sign of the supercritical magnetic state noted above. The surface magnetic relief of this film revealed with a scanning magnetic-force microscope has certain specific features (Fig. 3b). This picture consists of bright and dark bands and reflects a regular oscillation of the normal component of magnetization at a period of about 1 μm. This oscillation can be interpreted as the pres-

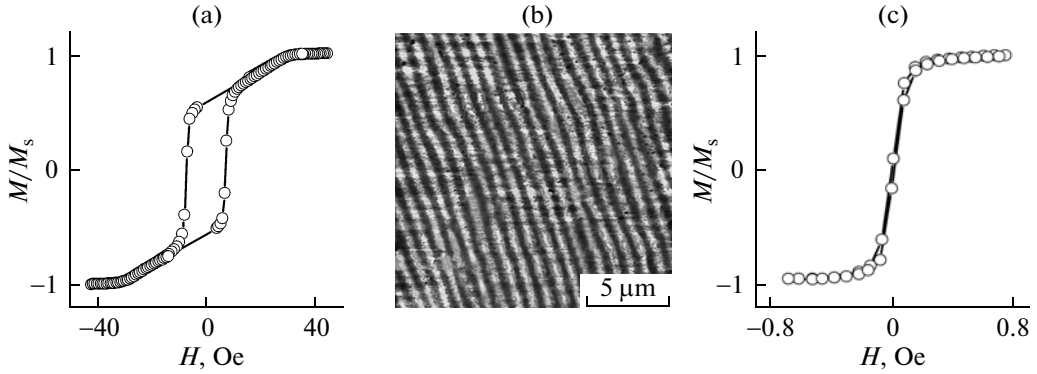

Fig. 3. (a, b) Longitudinal magnetometric hysteresis loops and the magnetic surface relief of an $Fe_{19}Ni_{81}$ film and (c) $Fe_{72.5}Cu_{1.1}Nb_{1.9}Mo_{1.5}Si_{14.2}B_{8.7}$ film.

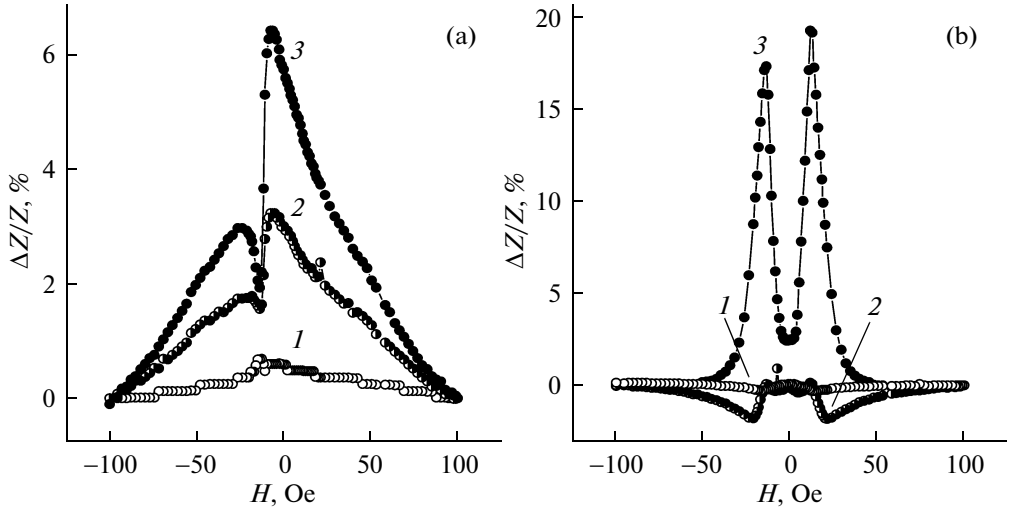

Fig. 4. Magnetic impedance of (a) $Fe_{19}Ni_{81}$ and (b) $Fe_{72.5}Cu_{1.1}Nb_{1.9}Mo_{1.5}Si_{14.2}B_{8.7}$ films at various probe current frequencies: (*1*) 50, (*2*) 175, and (*3*) 300 MHz.

ence of stripe domains, which is also a sign of the supercritical state.

The FM loop has another shape (Fig. 3c): it is close to a rectangular loop and has a very low coercive force (~0.1 Oe). Certain specific features of its shape (weak tilt, smooth change in the magnetization near magnetic saturation) can point to a small dispersion of the magnetic anisotropy. The main point is absent signs of the supercritical state; therefore, the films have no perpendicular anisotropy and, hence, columnar microstructure. This behavior is likely to be caused by hindered crystal formation, which is the basic feature of FINEMET alloys. According to X-ray diffraction data, the FM films have an amorphous structure and the PM films have a fine-grained crystalline structure.

To characterize the MI effect, we used the standard ratio

$$\frac{\Delta Z}{Z} = \frac{Z(H) - Z(H_{\max})}{Z(H_{\max})}100\%, \qquad (1)$$

where $H_{\max}$ is the maximum saturation field (in our case, 100 Oe). Figure 4 shows the ratio $\Delta Z/Z$ versus monotonically changing applied magnetic field H (MI curves) for film elements with homogeneous magnetic layers at various probe current frequencies f. Field H was applied along the long side of the element and was varied from +100 to −100 Oe. The MI effect is seen to be very weak in the PM element at relatively low frequencies f (Fig. 4a). As the frequency increases, this effect increases but is still very weak. Moreover, the MI loops are strongly asymmetric. These specific features are most likely to be caused by the supercritical state of the magnetic layers in the element. The MI curves of the FM elements are almost symmetric, but the MI effect is also low, at least at $f \le 300$ MHz. Since the supercritical state was not detected in the FM films, the low MI can be explained by the high electrical resistivity of the outer magnetic layers, which is inherent in an amorphous state. A probe current is likely to concentrate in a high-conductivity central layer, and its field does not provide significant dynamic permeability in the magnetic layers.

As noted above, one of the methods for preventing the formation of the supercritical state in the PM films

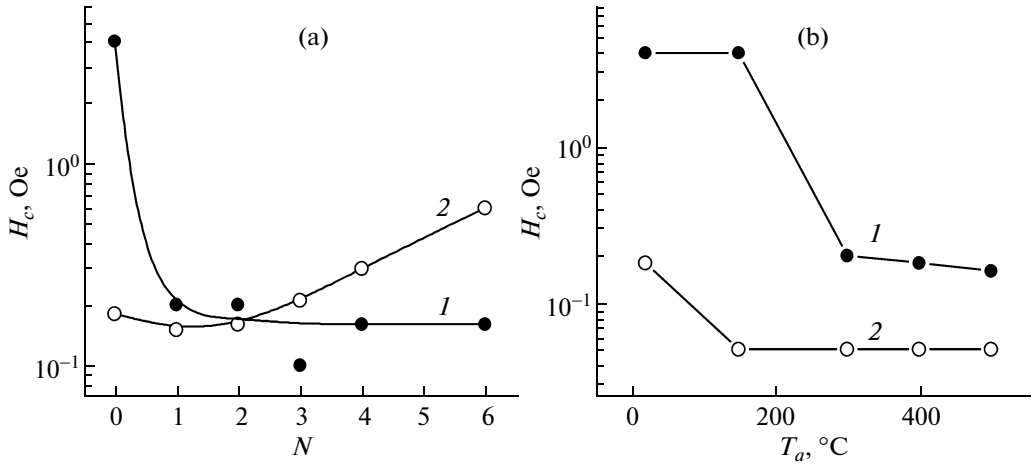

Fig. 5. Coercive force of (*1*) $Fe_{19}Ni_{81}$ or (*2*) $Fe_{72.5}Cu_{1.1}Nb_{1.9}Mo_{1.5}Si_{14.2}B_{8.7}$ film vs. (a) the number of Cu interlayers and (b) the annealing temperature.

is layered structuring. This process is assumed to be also effective for the FM film–based MI elements according to another cause. In this case, the role of high-conductivity layers can consist in the redistribution of current lines over the cross section of the elements. The effect of Cu interlayers on the magnetization reversal of the PM and FM films is illustrated in Fig. 5a, which shows the dependences of the coercive force determined from longitudinal hysteresis loops on the number of interlayers N. It is seen that the introduction of one interlayer into the PM films leads to a sharp decrease in H_c and that an increase in N does not change this property (curve *1*). In this case, the hysteresis loops become rectangular and stripe domains disappear. These findings indicate that the supercritical state does not exist in the structured films with magnetic layers thinner than 250 nm. The structuring affects the magnetization reversal of the FM films much more weakly (Fig. 5a, curve *2*). Nevertheless, H_c tends to increase with N, which can be related to an effective decrease in the magnetic layer thickness (see Fig. 2), and its value remains rather low.

Heat treatment, which is a traditional method for the modification of the microstructure of metals, can be considered as an alternative to structuring. In this work, we used steplike vacuum annealing of the films of both types. Figure 5b shows the dependences of the coercive force on annealing temperature T_{ann}. It is interesting that H_c of a PM film decreases sharply at $T_{ann} = 200$°C (curve *1*), which reflects the transition of the film from the supercritical state into a thin-film state (in which magnetization is located in the sample plane). Heat treatment also affects the properties of the FM film: H_c decreases noticeably at the first stage of annealing. In the case of PM films, the decomposition of the supercritical state can be attributed to the beginning of recrystallization; for the FM films, the decrease in H_c is likely to indicate the relaxation of nonuniform elastic stresses. Both factors improve the properties of the films as soft magnetic media. However, the heat treatment of three-layer MI elements is still disputable because of possible diffusion of Cu from the central layer to the adjacent magnetic layers and is to be studied separately [15]. In this work, we only noted this possibility and focused on the effects of structuring of MI elements.

Figure 6 shows the curves of the MI film elements whose magnetic layers contain four nonmagnetic interlayers. As is seen from a comparison with Fig. 4, structuring results in substantial changes in the properties of both the PM and FM elements, and the basic change consists in a multifold increase in the MI effect at all frequencies. The causes of these changes were actually discussed above and are thought to consist in the removal of the supercritical state in the magnetic PM layers and in a more efficient distribution of a probe current in the FM layers. Note also that the FM elements are characterized by relatively small peak widths in the MI curves, which indicates their higher selectivity and sensitivity to a magnetic field.

The conclusion about different mechanisms of the effect of structuring on the impedances of elements with different magnetic layers was supported by a numerical simulation performed with a finite element method and the FEMM software package [16]. We solved the problem of the dependence of active resistance R of a three-layer conductor on probe current frequency f at varied relative magnetic permeability μ and electrical conductivity σ during structuring of the outer layers. The sizes of the main layers in a model conductor coincided with the corresponding parameters of real film elements. The values of σ were chosen to be 4.6×10^7, 6.6×10^6, and 5.4×10^5 $(\Omega\ \mathrm{m})^{-1}$. These values reflected the properties of Cu and the PM and FM alloys, respectively. The change in the properties of the conductor in an applied magnetic field was taken into account by introducing two values of magnetic permeability, namely, $\mu_1 = 10$ and $\mu_2 = 500$.

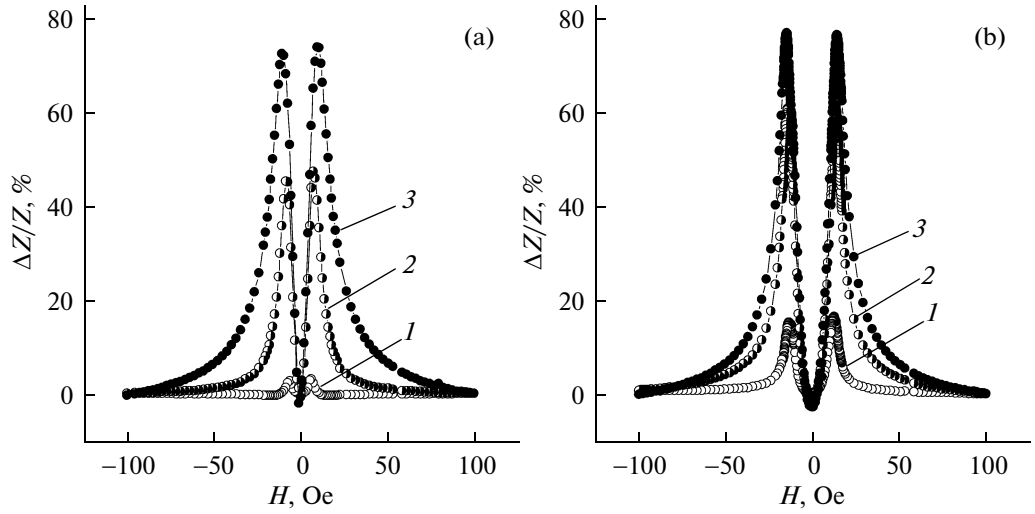

Fig. 6. Magnetic impedance of structured elements ($N = 4$) based on (a) $Fe_{19}Ni_{81}$ and (b) $Fe_{72.5}Cu_{1.1}Nb_{1.9}Mo_{1.5}Si_{14.2}B_{8.7}$ films at various probe current frequencies: (*1*) 50, (*2*) 175, and (*3*) 300 MHz.

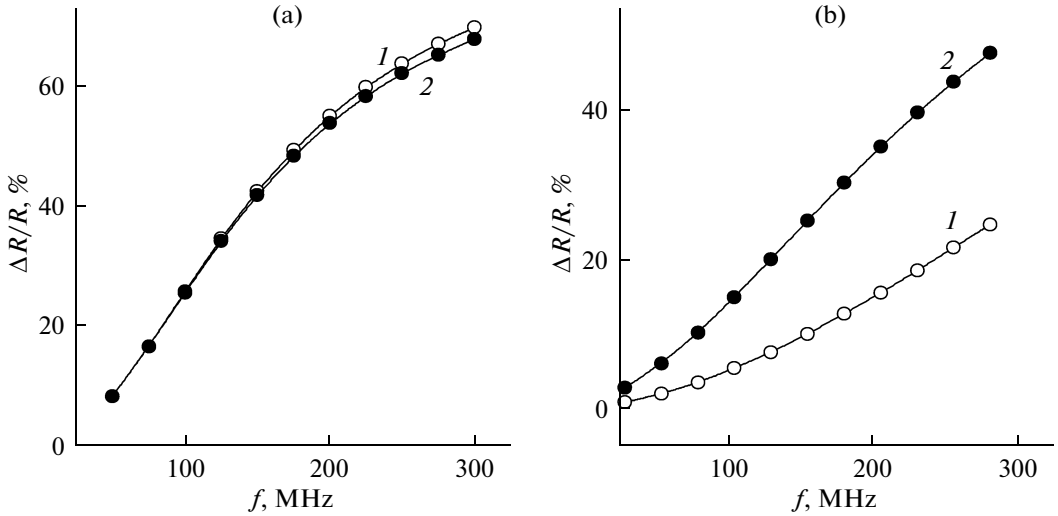

Fig. 7. Calculated frequency dependences of $\Delta R/R$ for film elements (*1*) without structuring interlayers and (*2*) with one structuring interlayer at the conductivity of the magnetic layers of (a) 6.6×10^6 and (b) 5.4×10^5 $(\Omega\ m)^{-1}$.

Figure 7 shows the results of simulation in the form of the frequency dependences of the ratio $\Delta R/R$ determined by the formula

$$\frac{\Delta R}{R} = \frac{R(\mu_2) - R(\mu_1)}{R(\mu_1)} \times 100\%. \qquad (2)$$

Curves *1* correspond to homogeneous outer layers of the elements, and curves *2*, to structured layers. We used the simplest version of structuring: one high-conductivity ($\sigma = 4.6 \times 10^7$ $(\Omega\ m)^{-1}$) interlayer 30 nm thick was introduced into the center of a magnetic layer. It is seen that structuring only weakly affects the properties of the elements with a relatively high conductivity of magnetic layers (analog of PM layers) and enhances $\Delta R/R$ for the case of layers with low σ (analog of FM layers). The experiment demonstrates that the main contribution to the magnetic impedance of the film elements under study is made by a change in its active component. Therefore, we may conclude that the model simulation agrees qualitatively with the experimental data for the FM elements and that the structuring effect for the PM elements consists in a change in their magnetic rather than electrical properties.

The positive effect of structuring raises the question of the optimal parameters of a fine structure. Some answers to this question can be found from an analysis of Fig. 8, which shows the frequency f dependences of the maxima in the MI curves for two types of elements with (curves *1*) nonstructured magnetic layers and with (curves *2*) 4 or (curves *3*) 16 interlayers. First, both types of elements demonstrate approximately the same maximum MI effect (about 75%) in the state with $N = 4$. Second, an increase in the number of interlayers

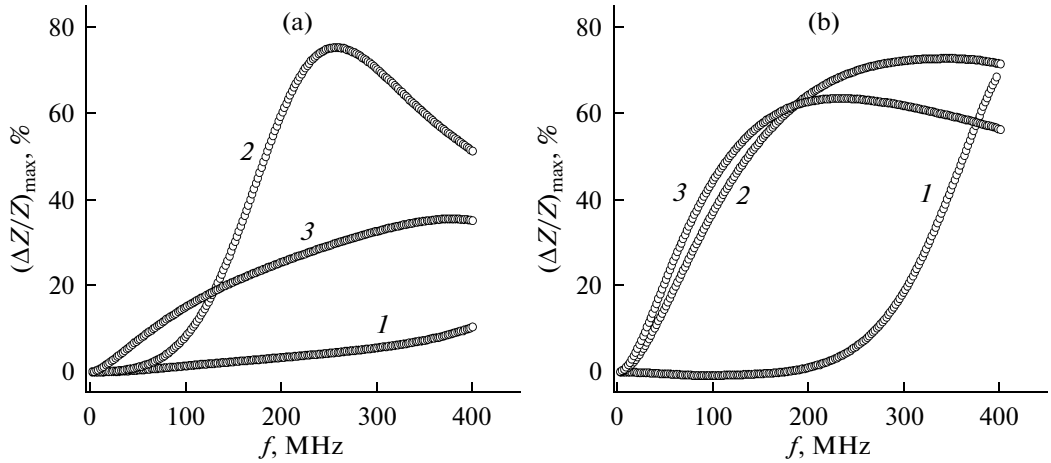

Fig. 8. Ratio $(\Delta Z/Z)_{max}$ vs. the probe current frequency for elements based on (a) $Fe_{19}Ni_{81}$ and (b) $Fe_{72.5}Cu_{1.1}Nb_{1.9}Mo_{1.5}Si_{14.2}B_{8.7}$ films at $N = (1)$ 0, (2) 4, and (3) 16 structuring interlayers.

decreases the maximum MI effect and increases its magnitude at relatively low frequencies. This behavior in the PM elements is most pronounced. Third, structured FM elements in the range $f < 200$ MHz exhibit a significantly higher MI effect than PM elements do.

CONCLUSIONS

Our results demonstrate the efficiency of application of layered structuring for improving the functional properties of film elements having magnetic impedance. The introduction of thin nonmagnetic and high-conductivity interlayers into magnetic layers prevents the formation of a columnar microstructure and, hence, perpendicular magnetic anisotropy in them and increases their conductivity. The former is important for permalloy-based elements, and the latter, for elements based on FINEMET-type amorphous alloys. A finer adjustment of the properties of elements with magnetic impedance is possible by optimizing the thickness parameters of the layered components and by combining structuring and low-temperature annealing.

ACKNOWLEDGMENTS

This work was supported by the Ministry of Education and Science of the Russian Federation (state contract no. 16.552.11.7020).

REFERENCES

1. M. Knobel, M. Vazquez, and L. Kraus, in *Handbook of Magnetic Materials*, Ed. by K. H. J. Buschow (North-Holland, Amsterdam, 2003), Vol. 15, pp. 497–563.
2. M.-H. Phan and H.-X. Peng, Prog. Mater. Sci. **53**, 323 (2008).
3. G. V. Kurlyandskaya, in *Encyclopedia of Sensors*, Ed. by C. A. Grimes and E. C. Dickey (American Scientific, New York, 2006), Vol. 4, pp. 205–237.
4. G. V. Kurlyandskaya and M. A. Cerdeira, in *Encyclopedia of Nanoscience and Nanotechnology*, Ed. by H. S. Nalwa (American Scientific, New York, 2011), Vol. 15, pp. 1–17.
5. F. Amalou and M. A. M. Gijs, J. Appl. Phys. **90**, 3466 (2001).
6. G. V. Kurlyandskaya, N. G. Bebenin, and V. O. Vas'kovskii, Fiz. Met. Metalloved. **111**, 136 (2011).
7. A. S. Antonov, S. N. Gadetskii, A. B. Granovskii, A. L. D'yachkov, V. P. Paramonov, N. S. Perov, A. F. Prokoshin, N. A. Usov, and A. N. Lagar'kov, Fiz. Met. Metalloved. **83** (6), 61 (1997).
8. Y. Sugita, H. Fujiwara, and T. Sato, Appl. Phys. Lett. **10**, 229 (1967).
9. M. A. Correa, A. D. C. Viegas, R. B. da Silva, A. M. H. de Andrade, and R. L. Sommer, Physica B **384**, 162 (2006).
10. N. Villar Alzola, G. V. Kurlyandskaya, A. Larrañaga, and A. V. Svalov, IEEE Trans. Magn. **48,** 1605 (2012).
11. G. V. Kurlyandskaya, A. V. Svalov, E. Fernández, A. Garcia-Arribas, and J. M. Barandiaran, J. Appl. Phys. **107**, 09C502 (2010).
12. S. O. Volchkov, E. Fernández, A. Garcia-Arribas, J. M. Barandiaran, V. N. Lepalovskij, and G. V. Kurlyandskaya, IEEE Trans. Magn. **47**, 3328 (2011).
13. L. V. Panina and K. Mohri, Sens. Actuators A **81**, 71 (2000).
14. G. V. Kurlyandskaya, J. L. Munoz, J. M . Barandiaran, A. Garca-Arribas, A. V. Svalov, and V. O. Vas'kovskiy, J. Magn. Magn. Mater. **242–245**, 291 (2002).
15. V. O. Vas'kovskii, V. N. Lepalovskii, and G. A. Galitskii, Fiz. Met. Metalloved. **82** (5), 83 (1996).
16. A. Garca-Arribas, J. M. Barandiaran, and D. de Cos, J. Magn. Magn. Mater. **320** (14), e4 (2008).

Translated by K. Shakhlevich